PAPER

Strong terahertz absorption in all-dielectric Huygens' metasurfaces

To cite this article: Michael A Cole *et al* 2016 *Nanotechnology* **27** 424003

IOP Publishing Nanotechnology
Nanotechnology 27 (2016) 424003 (6pp) doi:10.1088/0957-4484/27/42/424003

Strong terahertz absorption in all-dielectric Huygens' metasurfaces

Michael A Cole, David A Powell and Ilya V Shadrivov

Nonlinear Physics Centre and Centre for Ultrahigh Bandwidth Devices for Optical Systems (CUDOS), Research School of Physics and Engineering, The Australian National University, Canberra ACT 2601, Australia

E-mail: michael.cole@anu.edu.au

Received 7 April 2016, revised 27 July 2016
Accepted for publication 24 August 2016
Published 19 September 2016

Abstract

We propose an all dielectric metamaterial that acts as a perfect terahertz absorber without a ground plane. The unit cell consists of a dielectric cylinder embedded in a low index material. In order to achieve near-perfect terahertz absorption (99.5%) we employ impedance matching of the electric and magnetic resonances within the cylinders of the Huygens' metasurface. The impedance matching is controlled by changing the aspect ratio between the height and diameter of the cylinder. We show that the absorption resonance can be tuned to particular frequencies from 0.3 to 1.9 THz via changing the geometry of the structure while keeping a nearly constant aspect ratio of the cylinders.

Keywords: all-dielectric metamaterial, terahertz, Huygens' metasurface, perfect absorber, dielectric cylinders

(Some figures may appear in colour only in the online journal)

1. Introduction

Metamaterial research has yielded advances in devices for controlling wave transmission, reflection, and absorption from the optical to microwave wavelength ranges [1–5]. Perfect absorbers in the terahertz regime are a crucial step to unlock the potential of this region of the electromagnetic spectrum. The application of absorbers is very broad; for example, they are used in anti-reflective coatings and in detectors. This part of the spectrum still lacks efficient detectors and any detector of electromagnetic waves will require efficient absorbers. These devices will have uses in biomedical, security, and chemical sensing applications, as well as, wireless communication [6–8]. Currently, most metamaterial absorbers rely on layered metal–dielectric schemes and employ a metal ground plane to suppress transmission [6, 9–17] or patterned doped silicon structures [7, 8, 18] on large substrates. This results in very strong reflections at frequencies outside the absorption band. This problem was recently overcome at microwave frequencies, where strong absorption was achieved without a metal backing layer, by utilizing a racemic mixture of chiral particles [19].

Here we utilize the matched impedance of a dielectric Huygens' metasurface, [1, 20] which also eliminates the need for a backing metal ground plane. The relatively new concept of Huygens' metasurfaces have been employed to achieve perfect transmission and reflection [1, 2]; however, we used this novel idea to achieve perfect absorption. The benefits are that it allows for greater control of the wavefronts while requiring relatively simple geometric structures. First, we design absorbers by allowing for arbitrary material parameters and find what dielectric permittivity is required in order to achieve perfect absorption. Then we choose two real materials with parameters reasonably close to the optimal ones and design practically realizable absorbers with near perfect absorption. Compared to optical wavelengths, the terahertz domain offers larger possibilities for dielectric material selection because there are more materials with high permittivity.

2. Absorber design

Our proposed structure consists of an array of sub-wavelength dielectric cylinders embedded in a low-index medium, as

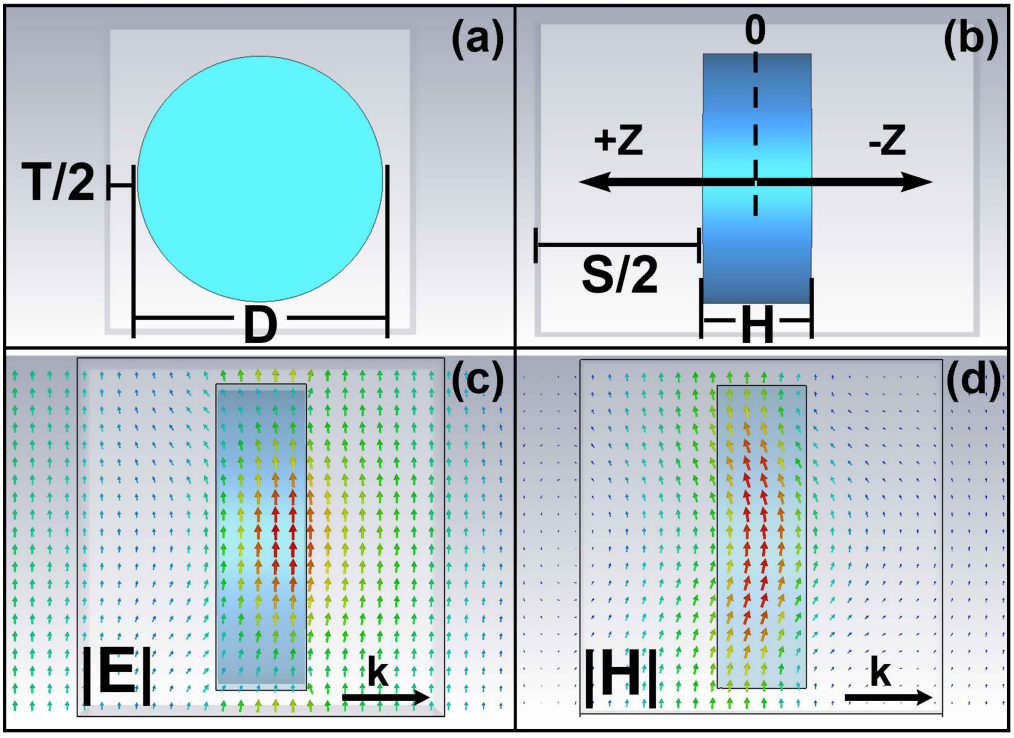

Figure 1. (a),(b) Schematic of the unit cell of our structure with a diameter (D), height (H), shift of cylinder (Z), distance between adjacent cylinders (T), and distance from cylinder surface to embedding material surface (S). Fields of the electric (c) and magnetic (d) dipole modes within the cylinder for frequencies of approximately 0.75 THz and 0.80 THz respectively, **k** indicates the direction of wave propagation, for $D = 200.0$ μm, $H = 60.03$ μm, $S = 182.66$ μm, and $T = 34.5$ μm, $Z = 0$.

shown in figure 1. Cylinders of finite height have magnetic and electric resonances with spectral locations which can be controlled by modifying their aspect ratio [1]. The use of dielectric structures is advantageous because they offer greater possibilities for material parameter selection and avoid the excessive dissipation of plasmonic metamaterials, which prevents good impedance matching. The parameters of the cylinders and embedding material are optimized so that the electric and magnetic resonances within the cylinders overlap and provide the best absorption. In this section we do not limit ourselves by choosing any particular materials for the cylinders and instead optimize for the material parameters that would be most suitable for absorbers.

All simulations in this work were performed using the CST Microwave Studio software package with unit cell boundary conditions enabled in the x- and y-directions and open (add space) boundary conditions in the z-direction. The terahertz signal is simulated by a default plane wave at normal incidence on the structures in the frequency domain solver. Finally, an adaptively refined tetrahedral mesh was applied to the simulated structures with an average size of 20 000 cells. A schematic of the unit cell of the structure can be seen in figures 1(a) and (b), the dimensions that were determined using the optimization feature of the CST Microwave Studio software package are labeled on the structure. Figure 1(a) shows the structure looking down the incident z-axis, D represents the diameter of the cylinder and T is the separation between adjacent cylinders. Figure 1(b) shows the side of the unit cell looking down the x-axis with the terahertz signal

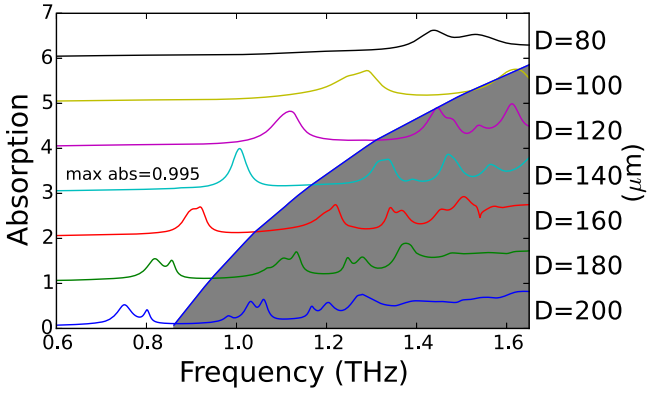

Figure 2. Absorption spectrum of the structures having different diameter cylinders. The overlap of the electric and magnetic resonances within the cylinder as the diameter of the cylinder changes while keeping the other parameters of the structure constant. Each simulated absorption spectrum is vertically displaced by 1 to clearly show the crossing of the resonances. The maximum absorption of approximately 99.5% occurs when the electric and magnetic resonances overlap at $D = 138.5$ μm. The shaded region contains higher order resonances which we do not consider here.

incident from left to right, here H is the height of the cylinder and Z refers to the possible offset of the resonators from the center of the embedding material, with the total thickness of the structure given by $S + H$. Figure 2 shows spectra for different values of D while keeping the quantities $H = 60.03$ μm, $S = 182.66$ μm, and $T = 34.5$ μm fixed. We focus on the two lowest order resonances, and to identify

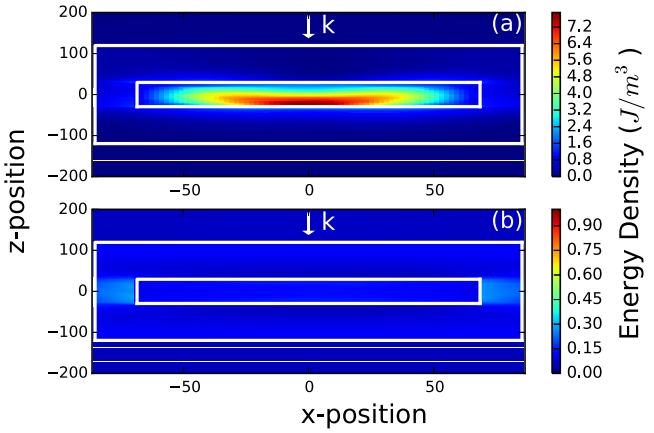

Figure 3. Panel (a) shows the electric energy density within the cylinder at peak absorption resonance, where **k** indicates the wave propagation direction. The white lines indicate the position of the cylinders within the center of the unit cell and outer embedding material. Panel (b) depicts the electric energy density within the structure that is much lower within the cylinder off peak resonance.

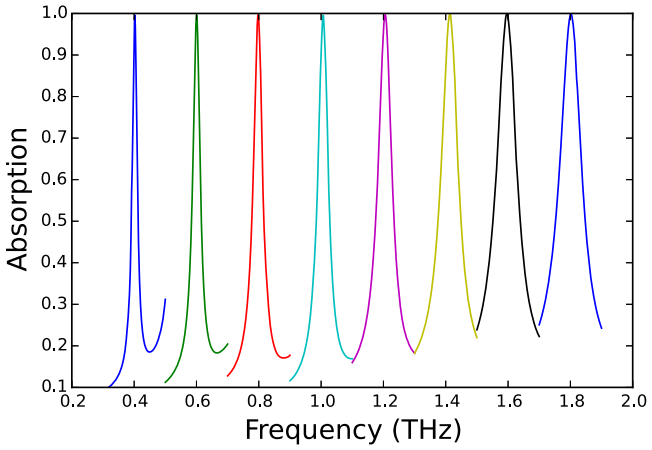

Figure 4. Numerical demonstration of near-perfect absorption at various frequencies within a wide frequency band by changing the geometry of the cylinders and surrounding structure. The aspect ratio of the cylinders is relatively constant throughout this process with a value of approximately 0.5, the corresponding parameters for each resonance are presented in figure 5.

them, we choose the curve at $D = 200$ μm, where these resonances are separated and plot their fields in figures 1(c) and (d). We see that the lower resonance is the electric dipole resonance within the cylinder corresponding to the peak frequency of approximately 0.75 THz in figure 2, the right resonant peak of the same curve in figure 2 corresponds to the magnetic resonance in figure 1(d) at a frequency of approximately 0.80 THz. Tuning these resonances to different frequencies by changing the dimensions of the structure offer great possibilities for spectrally-selective absorption and therefore, has potential for detection and imaging applications. The proposed absorption is based on a resonant effect; whereby, strong field localization and enhancement occurs within the dielectric cylinders. Figure 3(a) shows the localization of the electric energy density within the dielectric cylinder. The structures are optimized to achieve critical coupling, such that the radiation damping and internal dissipation rate are matched. For materials with low losses, this strong energy localization (and hence meeting the critical coupling condition) is accompanied by large energy storage in and around the resonator. This results in a high quality factor, hence strong absorption can only be achieved over a narrow bandwidth. This is demonstrated in figure 3(b), which shows that the stored energy within the cylinder is much weaker off resonance.

From figure 2 we see that the mutual position of the electric and magnetic resonances can be controlled, thus giving us great flexibility in designing the electromagnetic response of our metasurface. Now we proceed to find the structure parameters with highest absorption, to do this, we perform numerical simulations. The choice of embedding material becomes very important and the final material selected was polytetrafluoroethylene (PTFE or Teflon) [21, 22]. The values of the embedding material parameters $\epsilon = 2.09$ and a constant loss tangent of $\tan\delta = 0.007$ from the preceding references were fixed throughout the optimization processes discussed in the rest of this work and only the geometric parameters of the structure were optimized to achieve near-perfect absorption. The magnetic permeability for all materials in the simulations is set to a value of $\mu = 1$. It should be noted that normal incidence from the positive z-direction to the negative was the only case considered in this work.

At a chosen height of $H = 60.03$ μm and diameter of $D = 138.49$ μm the cylinder structure shows a near-perfect absorption of 0.995. Figure 2 shows the absorption resonances while keeping the height and all other parameters constant and only changing the diameter of the cylinder from 200.0 to 80.0 μm in increments of 20.0 μm. The period of the structures was chosen as $P = D + 34.5$ μm. It is seen that the resonances can cross each other as we change the diameter D, due to the orthogonality of the electric and magnetic dipole type modes. Near-perfect absorption is achieved when these modes overlap. Each spectrum in figure 2 has been offset vertically by progressively adding 1 to the absorption values for the sake of clarity.

The near-perfect absorption can also be tuned by slight changes in the material parameters of the structure while keeping a nearly constant aspect ratio (AR) of 0.5, where AR $= H/D$, where H and D are the height and diameter of the cylinder, respectively. Figure 4 shows the peak absorption at various frequencies in the region of 0.2–2.0 THz. In order to achieve perfect absorption, we used optimization algorithms of the CST and the permittivity of the cylinders was fixed at a value of 7.405. The loss tangent of the cylinders was kept constant at 0.032. Figure 5(a) shows the diameter and the height of the cylinders at each of the peak frequencies in figure 4(a). As the peak absorption frequency is shifted to higher frequencies the diameter (red dots) and the height (blue triangles) of the cylinders decreases. This is expected because at higher frequency and smaller wavelength one would expect the size of the structures to also decrease. Figure 5(b) shows the real (ϵ', green dots) and imaginary (ϵ'', black triangles)

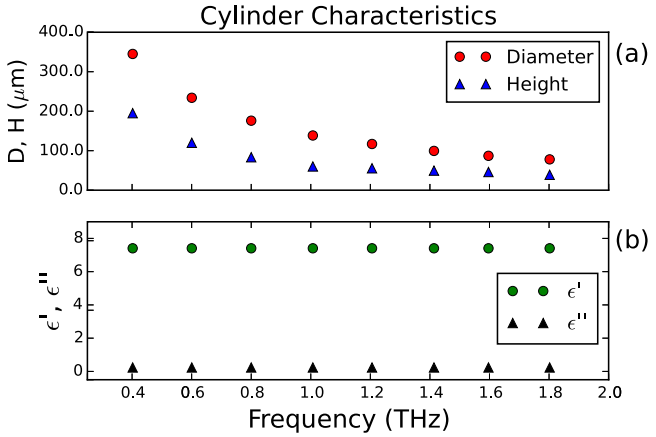

Figure 5. (a) The diameter (red dots) and height (blue triangles) of the cylinder for each peak in figure 4. As the frequency increases the diameter and height clearly decrease for this particular set of cylinder characteristics; however, the aspect ratio remains fairly constant at approximately 0.5. (b) Shows the real (green dots) and imaginary (black triangles) parts of the dielectric permittivity of the cylinders at each peak absorption frequency in figure 4. Both parts of the permittivity remain constant at each absorption frequency.

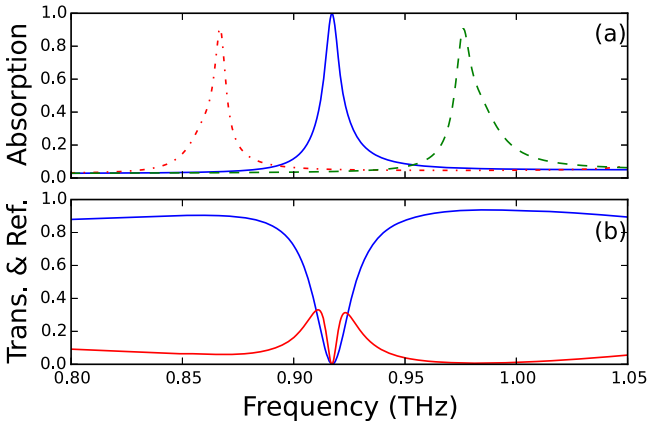

Figure 6. (a) Numerical results of the near-perfect absorption of quartz cylinders at 0.917 THz, blue curve. The red dashed–dotted and green dashed curves show the effects of changing the cylinder diameter by a factor of +10% and −10%, respectively. (b) High off-resonance transmission (blue) and relatively low reflection (red) throughout the simulated frequency range.

parts of the dielectric permittivity of the cylinders. The properties of the structure were optimized in the CST Microwave Studio simulations and the geometric parameters of the structure were changed to achieve perfect absorption. However, the real and imaginary parts of the permittivity remain constant.

Another important parameter that was found to be beneficial to the absorption optimization process is the shift of the cylinder from the center of the embedding material. The above optimization of our ideal structure was performed with $Z = 0$ as well as positive and negative shifts of the cylinder. Although we have only reported the data for zero shift of the ideal cylinder, Z was found to be crucial to the optimization of our realistic structures reported in the next section, when the physical material parameters are fixed.

3. Experimentally realizable systems

Since this approach to achieving strong absorption requires carefully selected material and geometric parameters, next we investigate whether these parameters can be realized with any existing materials. In order to make these simulations as realistic as possible, the permittivity of the embedding material was chosen to be $\epsilon = 2.09$ and a constant loss tangent of $\tan\delta = 0.007$. For the material of the cylinders, we found two promising examples based on published material data. Due to a lack of material data in the terahertz regime some of the best candidates for dielectric materials were crystals with anisotropic properties that were also taken into account in our simulations. Although the anisotropic properties of the materials introduce more complexity to the simulations we found that these properties did not hinder the performance of our absorbers.

3.1. Crystalline quartz

The first material investigated for near-perfect absorption was crystalline quartz. As it is a relatively weak absorber in the THz wavelength range, absorption resonances are expected to be narrow with high Q-factor. We assumed that the c-axis of the crystal is parallel to the cylinder axis. The electric permittivity used in the CST simulations, for quartz, for both the ordinary and extraordinary waves were estimated based on the data in plots in figure 5 of [23]. The aspect ratio of the quartz cylinders was 0.54 ($D = 150.0$ μm) with near-perfect absorption (0.998) at a frequency of 0.917 THz. The geometric properties of the embedding material were $T = 72.95$ μm for the separation of adjacent cylinders and $S = 120.85$ μm. The absorption of the quartz cylinders can be seen in figure 6(a). To study the effects of possible fabrication inaccuracies, the red dashed–dotted curve represents a plus 10% and the green dashed curve represents a minus 10% change in the diameter of the cylinders. This indicates that strong absorption is still achieved (>90%), even when deviating from the optimal geometric parameters; however, the frequency of the absorption is shifted. The near-perfect absorption is accompanied by relatively high transmission, >90% to the left and right of resonance shown in the center solid-blue curve in figure 6(b), this high transmission extends throughout the range 0.1–1.1 THz. The high transmission is also accompanied by relatively low reflection throughout the plotted frequency range off resonance. For the quartz metasurface, Z must be non-zero to achieve near perfect absorption. This asymmetry changes the ratio of electric and magnetic resonances within the cylinders and can be interpreted as introducing slight bianisotropy, which can be utilized to improve absorber performance [24]. This comes at the price of achieving near-perfect absorption only for waves incident from one side, although transmission is zero in both directions due to reciprocity.

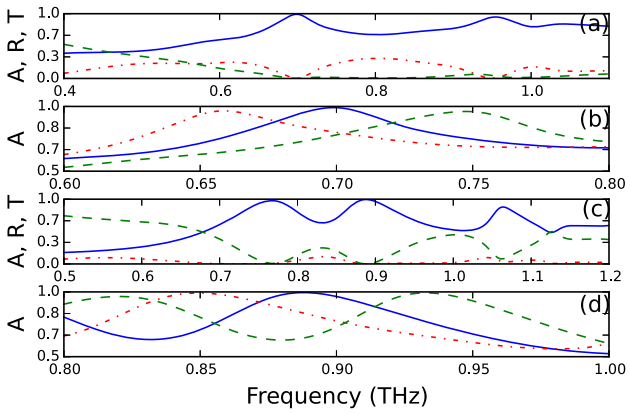

Figure 7. Absorption (A), Reflection (R) and Transmission (T). (a) The optimization of the dipole resonances of GaSe cylinders achieves an absorption of 0.996 at a frequency of 0.701 THz with the transmission (green dashed) and reflection (red dashed–dotted). (b) The blue solid curve is the zoomed in image of the first peak in panel (a), the red dashed–dotted and green dashed curves show the effects of changing the cylinder diameter by a factor of $+10\%$ and -10% respectively. (c) Numerical results of the near perfect absorption at 0.89 THz due to higher order resonance impedance matching, the transmission is the green dashed curve and reflection is the red dashed–dotted curve. (d) The blue solid curve is the zoomed in image of the second peak in panel (c), the red dashed–dotted and green dashed curves show the effects of changing the cylinder diameter by a factor of $+10\%$ and -10% respectively.

3.2. Gallium selenide

Gallium selenide (GaSe) is a material with considerably higher absorption in the THz range than quartz, thus it is expected to exhibit broader absorption resonances. The permittivity values for the ordinary wave were calculated based on the data presented in figure 2 of [25]. The measured values in the literature regarding the extraordinary wave are more convoluted but the values used in our simulations were estimated based on the values in [26, 27]. Figure 7(a) shows the highest absorption (blue curve) achieved in optimizing the absorption due to impedance matching of the dipole resonance within our GaSe metasurface. The highest absorption reached was 0.996, obtained at a frequency of 0.701 THz with an aspect ratio of 0.789 ($D = 186.0\ \mu$m). Unlike the quartz metasurface, GaSe has relatively low transmission (red dotted–dashed curve) and reflection (green dashed curve) off resonance. It should also be noted that in order to achieve the high absorption due to the impedance matching of the dipole resonances within the GaSe cylinders, the cylinder needed to be shifted by 30.47 μm toward the front of the structure. The values for T and S were 39.7 and 96.6 μm respectively. Similar to our analysis of the quartz metasurface, figure 7(b) shows the effects of possible fabrication inaccuracies, the red dashed–dotted curve represents a plus 10% and the green dashed curve represents a minus 10% change in the diameter of the cylinders. It is clear that the GaSe metasurface is more resilient to fabrication inaccuracies than the quartz metasurface because very strong absorption is still achieved ($>96.0\%$). GaSe has a considerably more complex dielectric anisotropic dispersion than quartz and both the real part and the imaginary parts of the permittivity for the ordinary and extraordinary waves are significantly higher. The increase in the real and imaginary parts of the permittivity has another unexpected effect on the absorption, one can clearly see higher order resonances around 0.95 THz in figure 7(a) that also present large absorption.

Just like the low order dipole resonances, these higher order resonances can interfere with each other to achieve impedance matching [28]. When considering the higher order resonances shown in figure 7(a) we found that the GaSe metasurface could also be optimized to achieve near-perfect absorption due to these higher order resonances. Figure 7(c) presents absorption over an extended frequency range (blue curve) to show the behavior of the metasurface off-resonance and that near perfect absorption (0.999) was found at 0.89 THz. The geometric parameters of the structure for perfect absorption were: $D = 114.07\ \mu$m, $H = 141.2\ \mu$m, $S = 124.4\ \mu$m, and $T = 121.7\ \mu$m. Unlike the first resonance of the metasurface, the transmission (green dashed curve) is not as low throughout the frequency range as it is at the first resonance but the reflection (red dashed–dotted curve) still remains relatively low off resonance. It is also interesting to note that this near perfect absorption was achieved for $Z = 0$ unlike with the dipole resonances in GaSe and quartz metasurfaces, thus there is no bianosotropy and the structure can act as a bi-directional absorber. The second resonance of the GaSe cylinders also has an added robustness to fabrication errors as is shown in figure 7(d), which is a zoomed in image of the central absorption peak in 7(c). The red dashed–dotted curve represents a $+10\%$ and the green dashed curve represents a -10% change in the diameter of the cylinder and the absorption is still near-perfect $>99.5\%$.

3.3. Potential fabrication challenges

There are some potential fabrication challenges that should be taken into account given these two materials. In both cases it should be noted that the dielectric properties appear to be highly dependent on the quality of the crystals produced. Furthermore, one of the many benefits of our structure is that the simplicity makes our design quite robust against fabrication inaccuracies. In addition, any differences in the permittivity of the experimental crystals produced from the values used in simulations can be overcome with the proper choice of geometric properties of the structure to achieve near-perfect absorption.

4. Conclusion

In this work we have proposed and simulated all-dielectric absorbers based on cylinders embedded in a low index material. These structures employ impedance matching of a Huygens' metasurface by overlapping the electric and magnetic resonances within the cylinders to achieve a near-perfect absorption in the terahertz regime. We have shown that with slight changes to the material used to create the cylinders and dimensions of the embedding material, the

frequency of perfect absorption can be tuned throughout the terahertz region. Finally, we demonstrated near perfect absorption in two possible materials that could be used to fabricate the cylinders using dielectric parameters found in the current literature. We have shown that quartz can be used for creating relatively narrow absorption resonances, while GaSe structures can demonstrate broadband bi-directional absorption. Both considered materials have anisotropic properties, therefore our approach can be applied to both isotropic and anisotropic materials. Our structure has a wide use of possible applications in detectors or imaging of terahertz radiation while eliminating the drawbacks of plasmonic devices.

Acknowledgments

This work was supported by the Australian Research Council (CUDOS Centre of Excellence CE110001018).

References

[1] Staude I *et al* 2013 *ACS Nano* **7** 7824–32
[2] Moitra P, Slovick B A, Yu Z G, Krishnamurthy S and Valentine J 2014 *Appl. Phys. Lett.* **104** 171102
[3] Slovick B, Yu Z G, Berding M and Krishnamurthy S 2013 *Phys. Rev.* B **88** 165116
[4] Landy N I, Sajuyigbe S, Mock J J, Smith D R and Padilla W J 2008 *Phys. Rev. Lett.* **100** 207402
[5] Ra'di Y, Simovski C R and Tretyakov S A 2015 *Phys. Rev. Appl.* **3** 037001
[6] Grbovic D, Alves F, Kearney B, Waxer B, Perez R and Omictin G 2013 *J. Micro/Nanolithogr. MEMS MOEMS* **12** 041204
[7] Withayachumnankul W, Shah C M, Fumeaux C, Ung B S Y, Padilla W J, Bhaskaran M, Abbott D and Sriram S 2014 *ACS Photonics* **1** 625–30
[8] Cheng Y Z, Withayachumnankul W, Upadhyay A, Headland D, Nie Y, Gong R Z, Bhaskaran M, Sriram S and Abbott D 2015 *Adv. Opt. Mater.* **3** 376–80
[9] Tao H, Landy N I, Bingham C M, Zhang X, Averitt R D and Padilla W J 2008 *Opt. Express* **16** 7181–8
[10] Zhu J, Ma Z, Sun W, Ding F, He Q, Zhou L and Ma Y 2014 *Appl. Phys. Lett.* **105** 021102
[11] Liu S, Chen H and Cui T J 2015 *Appl. Phys. Lett.* **106** 151601
[12] Kearney B, Alves F, Grbovic D and Karunasiri G 2013 *Opt. Mater. Express* **3** 1020–5
[13] Xu B, Gu C, Li Z and Niu Z 2013 *Opt. Express* **21** 23803–11
[14] Chen H T 2012 *Opt. Express* **20** 7165–72
[15] Wang B X, Zhai X, Wang G Z, Huang W Q and Wang L L 2015 *Opt. Mater. Express* **5** 227–35
[16] Wen Q Y, Xie Y S, Zhang H W, Yang Q H, Li Y X and Liu Y L 2009 *Opt. Express* **17** 20256–65
[17] Guo Y, Yan L, Pan W, Luo B and Luo X 2014 *Plasmonics* **9** 951–7
[18] Shi C, Zang X, Wang Y, Chen L, Cai B and Zhu Y 2014 *Appl. Phys. Lett.* **105** 031104
[19] Asadchy V S, Faniayeu I A, Radi Y, Khakhomov S A, Semchenko I V and Tretyakov S A 2015 *Phys. Rev.* X **5** 031005
[20] Decker M, Staude I, Falkner M, Dominguez J, Neshev D N, Brener I, Pertsch T and Kivshar Y 2015 *Adv. Opt. Mater.* **3** 813–20
[21] Cunningham P D, Valdes N N, Vallejo F A, Hayden L M, Polishak B, Zhou X H, Luo J, Jen A K Y, Williams J C and Twieg R J 2011 *J. Appl. Phys.* **109**
[22] Jin Y S, Kim G J and Jeon S G 2006 *J. Korean Phys. Soc.* **49** 513–7
[23] Grischkowsky D, Keiding S, van Exter M and Fattinger C 1990 *J. Opt. Soc. Am.* B **7** 2006–15
[24] Yazdi M, Albooyeh M, Alaee R, Asadchy V, Komjani N, Rockstuhl C, Simovski C R and Tretyakov S 2015 *IEEE Trans Antennas Propag.* **63** 3004–15
[25] Yu B L, Zeng F, Kartazayev V, Alfano R R and Mandal K C 2005 *Appl. Phys. Lett.* **87** 182104
[26] Molloy J F, Naftaly M, Andreev Y, Kokh K, Lanskii G and Svetlichnyi V 2014 *Opt. Mater. Express* **4** 2451–9
[27] Chen C W, Tang T T, Lin S H, Huang J Y, Chang C S, Chung P K, Yen S T and Pan C L 2009 *J. Opt. Soc. Am.* B **26** A58–65
[28] Kruk S, Hopkins B, Kravchenko I I, Miroshnichenko A, Neshev D N and Kivshar Y S 2016 *APL Photonics* **1** 030801